

The average X-ray/gamma-ray spectrum of radio-quiet Seyfert 1s

Dorota Gondek¹, Andrzej A. Zdziarski^{1,2}, W. Neil Johnson³, Ian M. George^{4,5}, Kellie McNaron-Brown⁶, Paweł Magdziarz⁷, David Smith⁸ and Duane E. Gruber⁹

¹*N. Copernicus Astronomical Center, Bartycka 18, 00-716 Warsaw, Poland; Internet: (dorota, aaz)@camk.edu.pl*

²*Institute for Theoretical Physics, University of California, Santa Barbara, CA 93106, USA*

³*E. O. Hulburt Center for Space Research, Naval Research Laboratory, Washington, DC 20375, USA*

⁴*Laboratory for High Energy Astrophysics, Code 660.2, NASA/Goddard Space Flight Center, Greenbelt, MD 20771, USA*

⁵*Universities Space Research Association, USA*

⁶*George Mason University, Fairfax, VA 22030, USA*

⁷*Astronomical Observatory, Jagiellonian University, Orla 171, 30-244 Cracow, Poland*

⁸*Department of Physics, University of Leicester, University Road, Leicester LE1 7RH, UK*

⁹*Center for Astrophysics and Space Science, University of California at San Diego, La Jolla, CA 92093, USA*

28 September 2018

ABSTRACT

We have obtained the average 1–500 keV spectrum of radio-quiet Seyfert 1s using data from *EXOSAT*, *Ginga*, *HEAO-1*, and *GRO OSSE*. The spectral fit to the combined average *EXOSAT* and OSSE data is fully consistent with that for *Ginga* and OSSE, confirming results from an earlier *Ginga*/OSSE sample. The average spectrum is well-fitted by a power-law X-ray continuum with an energy spectral index of $\alpha \simeq 0.9$ moderately absorbed by an ionized medium and with a Compton reflection component. A high-energy cutoff (or a break) in the the power-law component at a few hundred keV or more is required by the data. We also show that the corresponding average spectrum from *HEAO-1* A1 and A4 is fully compatible with that obtained from *EXOSAT*, *Ginga* and OSSE. These results confirm that the apparent discrepancy between the results of *Ginga* (with $\alpha \simeq 0.9$) and the previous results of *EXOSAT* and *HEAO-1* (with $\alpha \simeq 0.7$) is indeed due to ionized absorption and Compton reflection first taken into account for *Ginga* but not for the previous missions. Also, our results confirm that the Seyfert-1 spectra are on average cut off in γ -rays at energies of at least a few hundred keV, *not* at ~ 40 keV (as suggested earlier by OSSE data alone). The average spectrum is compatible with emission from either an optically-thin relativistic thermal plasma in a disk corona, or with a nonthermal plasma with a power-law injection of relativistic electrons.

Key words: galaxies: active – galaxies: Seyfert – X-rays: galaxies – gamma-rays: observations – gamma-rays: theory – accretion, accretion disks

1 INTRODUCTION

The average X-ray/ γ -ray (hereafter $X\gamma$) spectra of Seyfert 1s and 2s observed by both *Ginga* and *GRO OSSE* have recently been obtained by Zdziarski et al. (1995, hereafter Z95). The main result of that study for Seyfert 1s is that their average spectral high-energy cutoff is around several hundred keV. This is thus similar to the cutoff of IC 4329A, a bright Seyfert 1 (Madejski et al. 1995; Zdziarski et al. 1994, hereafter Z94). Z95 also found that the average spectrum of radio-quiet (hereafter RQ) Seyfert 1s has the energy spectral

index of $\alpha \simeq 0.9$ as well as a Compton-reflection component, as previously obtained for *Ginga* spectra alone (Pounds et al. 1990; Nandra & Pounds 1994, hereafter NP94). However, since the 23 *Ginga* and 8 OSSE observations of RQ Seyfert 1s used in Z95 are not simultaneous and that sample consists of only 4 objects, there is a clear need to confirm those results using enlarged and independent samples.

Here, we test and confirm the results of Z95 using spectra of RQ Seyfert 1s from *EXOSAT*, *HEAO-1*, *Ginga*, and OSSE. [Discussion of the average $X\gamma$ properties of radio-loud Seyferts is given in Woźniak et al. (1996).] We obtain

the average spectrum of RQ Seyfert 1s detected by both *EXOSAT* and OSSE, a sample which consists of 7 objects. The objects were observed 41 times by *EXOSAT* and 18 times by OSSE. Averaging this large numbers of observations is expected to compensate for the lack of simultaneity of the observations. We also obtain the corresponding average spectrum from *HEAO-1* A1 and A4. Furthermore, we analyze the *Ginga*/OSSE sample enlarged by new OSSE observations of NGC 5548 and with addition of NGC 7469.

After presenting the spectra, we study physical processes that can be responsible for the observed X γ emission. We consider both thermal and nonthermal plasmas.

2 THE DATA

We use *EXOSAT* spectra from the HEASARC archive with the quality flag 3 or higher (which indicates observations with relatively reliable background subtraction) of RQ Seyfert 1s detected by OSSE. We exclude the Seyfert 1s brightest in X-rays, NGC 4151 and IC 4329A, in order to avoid their dominance of the co-added spectrum. The usable *EXOSAT* energy range is from 1.2 keV to 8 keV (channels 6–31). The spectra above 8 keV suffer from relatively inaccurate global background subtraction [as opposed to local background subtraction used by, e.g., Turner & Pounds (1989)]. The individual spectra include a 1 per cent systematic error. The spectra from *EXOSAT* (as well as *Ginga* and *HEAO-1*) are co-added with the weights corresponding to the length of time of each observation. Both the counts and the response matrices for each *EXOSAT* observation are added using a procedure (specially written for *EXOSAT* data) in the FTOOLS data processing package.

The OSSE spectra take into account an estimated systematic error correction to the spectra [see, e.g., Zdziarski, Johnson & Magdziarz (1996) for details]. We use the OSSE response matrix as revised in 1995, which results in the 50–60 keV fluxes about 20 per cent higher than in the earlier response (used, e.g., in Z95).

The *EXOSAT*/OSSE sample consists of 7 RQ Seyfert 1s [41, 18] (the numbers in brackets give the number of *EXOSAT* and OSSE observations, respectively): MCG –6-30-15 [4, 2], Mrk 509 [3, 2], NGC 3783 [4, 1], NGC 5548 [11, 6], MCG 8-11-11 [10, 2], ESO 141-55 [2, 2], and NGC 7469 [7, 3].

We also use the average spectrum in the 2–180 keV range from observations by *HEAO-1* A1 and A4 (Wood et al. 1984; Rothschild et al. 1983). [We do not use *HEAO-1* A2 data because the normalization of archival spectra is not known (Weaver, Arnaud & Mushotzky 1995).] The A4 spectra of individual objects have been recreated using the current version of the instrument software. In the 2–10 keV energy range, we use the *HEAO-1* A1 data as published by Wood et al. (1984). Since that detector provides no spectral information and only instrumental counts are given in Wood et al. (1984), we have obtained the 2–10 keV fluxes using the counts-to-flux conversion as given for the Crab. In order to get an estimate of the 2–10 keV average spectrum, we use the average overall slope in that range of $\alpha = 0.7$ (see Section 4 below).

Our *Ginga* data are the same as those for Seyfert 1s in Z95 except for the addition of NGC 7469 (NP94). The

Ginga/OSSE sample thus consists of 5 RQ Seyfert 1s [25, 14] (the numbers in brackets give the number of *Ginga* and OSSE observations, respectively): MCG –6-30-15 [4, 2], Mrk 509 [4, 2], NGC 3783 [1, 1], NGC 5548 [14, 6], and NGC 7469 [2, 3]. We have obtained the average spectra for both the top-layer and the mid-layer *Ginga* data (Turner et al. 1989). However, we have found that the mid-layer spectrum above 10 keV is systematically softer than the corresponding top-layer spectrum. Since the mid-layer calibration is much more uncertain than that of the top layer (Turner et al. 1989), we use in this paper only the top-layer data. We use the energy range of 1.7–18 keV (channels 4–31), for which the instrumental background subtraction is accurate. As in Z95, a 0.5 per cent systematic error correction has been applied to the co-added *Ginga* spectrum.

3 MODEL

In our fits, we use the XSPEC spectral fitting package version 9.0 (Arnaud 1996). As in Z95, we model the underlying continuum as a power law with an exponential cutoff at an energy, E_c . Z95 found that ionized low-energy absorption is necessary to explain the average *Ginga* spectrum of Seyfert 1s. Thus, we model absorption as due to an ionized medium with the abundances from Anders & Ebihara (1982) and the ion opacities of Reilman & Manson (1979) except for the Fe K-edge energies, for which results of Kaastra & Mewe (1993) were used. The absorber temperature is assumed to equal $T = 10^5$ K (Krolik & Kallman 1984), its column density is N_H , and an ionization parameter is defined by $\xi = L/(nr^2)$. Here L is the 5 eV–20 keV luminosity in a power law spectrum with the average energy index of 0.7, and n is the density of the absorber located at distance r from the illuminating source. Model parameters are given at the average redshift for each sample, $\langle z \rangle$. In addition to the ionized absorber, we include a fixed neutral absorber at $z = 0$ with $N_{H,G}$ equal to the average Galactic value for each sample.

The underlying continuum irradiates cold matter, e.g., an accretion disk, and gives rise to a Compton-reflection spectral component (Lightman & White 1988). Differently from Z95, who used the reflection spectrum averaged over all the angles of the reflected photons (Lightman & White 1988), we assume a viewing angle of 30° [corresponding to an orientation close to face-on expected in type-1 AGNs, Antonucci (1993)]. We use the angle-dependent reflection Green’s functions of Magdziarz & Zdziarski (1995). The luminosity intercepted by the reflecting medium equals R (the relative contribution of reflection) times the luminosity emitted outward, i.e., $2\pi R$ gives the solid angle subtended by the absorber as seen from the source of the incident radiation. The continuum reflection is accompanied by emission of a fluorescent Fe K α line, which we model here as a Gaussian at an energy E_{Fe} and the width σ_{Fe} .

4 RESULTS

We first study the *Ginga*/OSSE average spectrum, using the sample enlarged with respect to that in Z95 (see Section 2). The data and the best-fit model are shown in Fig. 1a. The fit parameters are given in Table 1. We obtain $\alpha \simeq 0.90 \pm 0.05$

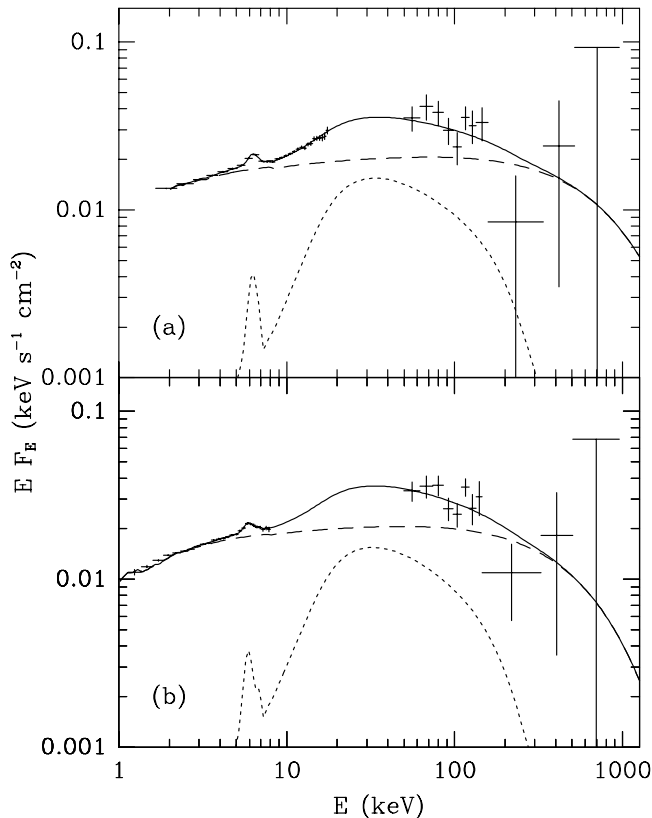


Figure 1. The average spectrum (*crosses*) of RQ Seyfert 1 galaxies from *Ginga*/OSSE (a) and *EXOSAT*/OSSE (b). The upper limits here and in figures below are $2\text{-}\sigma$. The dashed curves represent power-law spectra with exponential cutoffs and bound-free absorbed at low energies, and the dotted curves represent Compton reflection including the Fe $K\alpha$ line. The solid curves give the sum.

and the e -folding energy between ~ 0.4 MeV and 2.7 MeV, which is in agreement with Z95. The relative contribution of reflection, $R \simeq 0.76 \pm 0.15$ is about 2/3 of that found by Z95, which is explained by the angle-dependent reflection spectrum at 30° both having a higher normalization with respect to the underlying continuum and being harder in the $\sim 10\text{--}30$ keV range than the angle-averaged reflection spectrum (Magdziarz & Zdziarski 1995). [Note that this effect will also reduce large values of angle-averaged R obtained by Weaver et al. (1995) for Seyfert 1s observed by *HEAO-1* A2.] Our values of α and R are in agreement with the average values for *Ginga* of NP94, $\alpha \simeq 0.95$ with a dispersion of 0.15 and $R \sim 0.5\text{--}0.7$. The equivalent width of the $K\alpha$ line is 120^{+40}_{-40} eV, which agrees with the value expected from fluorescence in the reflecting medium at our R (George & Fabian 1991). We have also confirmed that our results are only weakly dependent on the (relatively uncertain) elemental abundances. When the abundances of Anders & Ebihara (1982) are replaced by those of Anders & Grevesse (1989) (with higher abundances of metals, in particular with about 40 per cent more Fe), our results change only slightly. E.g., marginally more Compton reflection is obtained, $R = 0.80^{+0.16}_{-0.14}$ ($\chi^2 = 71.8/72$ dof).

Then we consider the *EXOSAT*/OSSE sample, see Fig.

1b. Since the usable *EXOSAT* spectrum extends only to 8 keV, Compton reflection is not constrained. Therefore, we fix R at the value obtained from the *Ginga*/OSSE average. The equivalent width of the $K\alpha$ line obtained, 100^{+100}_{-50} eV, is consistent with this assumption. (The best-fit line energy is 5 per cent less than that for *Ginga*, which is due to a gain inaccuracy of *EXOSAT*.) Furthermore, we find that there is an apparent soft X-ray excess present in the average spectrum below 2 keV, a feature common in Seyfert 1 spectra (Wilkes & Elvis 1987; Turner & Pounds 1988). Rather than add a separate spectral component (which would be poorly constrained by our data), we fit only the spectrum above 2 keV. We show, however, the spectrum below 2 keV in Fig. 1b.

We find that the fit parameters of the *EXOSAT*/OSSE average spectrum are virtually identical to those for the *Ginga*/OSSE average. The two spectra are compared in Fig. 2. We thus confirm that the average value of the e -folding energy in the spectra of Seyfert 1s is several hundred keV rather than ~ 40 keV (Johnson et al. 1994). The latter value was obtained using narrow-band OSSE data only, neglecting Compton reflection, using a spectral model implying X-ray power laws much harder than observed, as well as with the old OSSE response. Those factors fully explain the discrepancy.

We point out that the OSSE spectra of individual Seyferts appear more uniform (Johnson et al. 1994) than their X-ray spectra, for which the $1\text{-}\sigma$ dispersion of α is 0.15 ± 0.04 (NP94). If indeed AGNs with different α have similar γ -ray spectra, there will be a positive correlation of E_c with α , rather than a constancy of E_c among objects with different α (because harder X-ray spectra will need to be cut off stronger than softer ones in order to yield similar spectra above 50 keV). The range of E_c among individual AGNs will be then larger than that given in Table 1, which range corresponds to our *average* X-ray spectrum, with $\alpha = 0.90 \pm 0.05$. This appears to be confirmed for NGC 4151, a bright Seyfert with a hard X-ray spectrum. Zdziarski et al. (1996) have found no statistical difference between the shape of the spectra of NGC 4151 from four OSSE observations during 1991–93 and the average OSSE spectrum of the Seyfert 1s observed by *EXOSAT*. However, the e -folding energy for NGC 4151 is $E_c \simeq 150$ keV (below the range of E_c in Table 1) as a consequence of $\alpha \simeq 0.7$ [for the cut-off power-law model with reflection fitted to 1991 June *Ginga*/OSSE observation (Zdziarski et al. 1996)].

The agreement between the average *EXOSAT* and *Ginga* spectra confirms that the average value of $\alpha \simeq 0.7$ for Seyferts found based on *EXOSAT* observations (Turner & Pounds 1989) is indeed an artifact of assuming neutral absorption and not including Compton reflection. When both effects are included, the average $\alpha \simeq 0.9$ for both *EXOSAT* and *Ginga*.

A similar average spectral index of $\alpha \simeq 0.6\text{--}0.7$ was also obtained by *HEAO-1* (Rothschild et al. 1983; Mushotzky 1984). Here, we obtained the average *HEAO-1* A1/A4 spectrum for the objects in the *EXOSAT*/OSSE sample (see Section 2), shown as dotted symbols in Fig. 2. We see that apart from a small difference in the normalization the two spectra are fully consistent with each other. Thus, the spectra of Seyfert 1s from *EXOSAT* and *HEAO-1* are compatible with an intrinsic power law with $\alpha \simeq 0.9$. Our average *HEAO-1*

Table 1. Parameters of the spectral fits to the average RQ Seyfert 1 spectrum. The *Ginga*/OSSE and *EXOSAT*/OSSE samples are denoted by ‘GO’ and ‘EO’, respectively. The symbols are explained in the text. Parameters with no error ranges are fixed. N_{H} are in units of 10^{21} cm^{-2} , E_c , E_{Fe} , and σ_{Fe} are in keV. Errors are for 90 per cent confidence limit based on a $\Delta\chi^2 = 2.7$ criterion (Lampton, Margon & Bowyer 1976).

Data	$\langle z \rangle$	α	E_c	R	$N_{\text{H,G}}$	N_{H}	ξ	E_{Fe}	σ_{Fe}	χ^2/dof
GO	0.017	$0.90^{+0.05}_{-0.05}$	730^{+1950}_{-340}	$0.76^{+0.15}_{-0.15}$	0.5	32^{+19}_{-19}	530^{+310}_{-300}	$6.32^{+0.15}_{-0.16}$	$0.33^{+0.28}_{-0.33}$	74.1/72
EO	0.020	$0.90^{+0.09}_{-0.07}$	510^{+4300}_{-250}	0.76	0.7	16^{+24}_{-14}	140^{+340}_{-140}	$6.0^{+0.2}_{-0.2}$	$0.3^{+0.5}_{-0.3}$	73.3/67

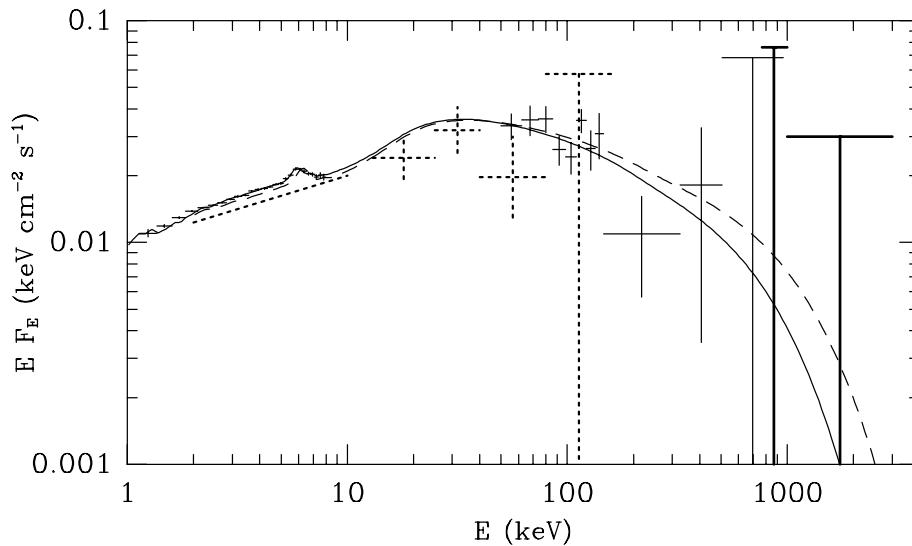


Figure 2. Comparison of the estimates of the average spectrum of RQ Seyfert 1s obtained with various instruments. The solid-line data are from *EXOSAT* and OSSE. The solid and dashed curves are the best-fit models for the *EXOSAT*/OSSE and *Ginga*/OSSE samples, respectively. Note that the two curves have the actual normalizations from the fits. The agreement between the two spectra confirms that the X-ray variability of the AGNs is indeed fully compensated by the sizes of the samples. The dotted symbols represent the average *HEAO-1* A1 and A4 spectrum, which is in agreement with the *Ginga*/*EXOSAT*/OSSE spectrum. The thick-line upper limits are for combined emission of all Seyfert galaxies observed by COMPTEL (Maisack et al. 1995).

spectrum is almost the same as that obtained for a larger sample of Seyfert 1s by Maisack, Wood & Gruber (1994).

Fig. 2 also shows the upper limits on emission of *all* Seyferts observed by COMPTEL (Maisack et al. 1995). The corresponding upper limits for the *EXOSAT*/OSSE sample of RQ Seyfert 1s are about 3–4 times higher. We see that even the limits for all Seyferts do not provide additional constraints on our average spectrum. The upper limits on γ -ray emission of Seyferts were also obtained by EGRET for energies above 100 MeV (Lin et al. 1993). The weighted 2- σ upper limit for the *EXOSAT*/OSSE sample corresponds to $E F_E \lesssim 0.004 \text{ keV cm}^{-2} \text{ s}^{-1}$ at 100 MeV. This is much above our extrapolated models. However, that upper limit does rule out an extrapolation of the $\alpha = 0.9$ power law *without* a break up to 100 MeV, at which energy the extrapolated power law spectrum would be a factor of ~ 5 above the upper limit. Thus, the EGRET results provide a confirmation of the existence of a high-energy spectral break in Seyferts, independent of the OSSE results.

5 PHYSICAL PROCESSES IN SEYFERTS

5.1 Thermal models

Exponentially cut-off power-laws (used here to fit the average Seyfert-1 spectrum) can be used to model spectra due to Comptonization in thermal, optically-thin, mildly-relativistic plasmas (e.g., Z94). The parameters, α and E_c , can be related to the Thomson optical depth, τ , and temperature, T . For $E_c = 400 \text{ keV}$, which fits both our average spectra and IC 4329A, Z94 find $E_c \simeq 1.6kT$ (implying $kT \simeq 260 \text{ keV}$). Z94 also provide an expression for $\alpha(\tau, kT)$ in a slab geometry, which yields $\tau \simeq 0.1$ for $\alpha = 0.95$, $E_c = 400$. Thus, optically-thin, mildly relativistic plasmas can explain the observed spectra of Seyfert 1s. The large values of E_c obtained here rule out models with Comptonization in optically thick plasmas (Sunyaev & Titarchuk 1980), used in the past to fit Seyfert-1 spectra (e.g., Miyoshi et al. 1988).

Haardt & Maraschi (1993) have proposed that the hot plasma in Seyferts forms a corona above the surface of an accretion disk, and that most of the energy dissipation occurs in the corona. Then the plasma temperature can be determined from the disk-corona energy balance, which makes the model more self-consistent. The disk-corona model also accounts for the Compton-reflection spectral components in the spectra of RQ Seyfert 1s. Z94 found that the best-fit

parameters of the X γ spectrum of IC 4329A satisfy that energy balance, i.e., the hard corona emission reprocessed by the disk self-consistently provides the seed of soft photons (in the UV range) for Compton upscattering into the hard spectrum.

Those results have recently been confirmed by a more sophisticated treatment of the radiative transfer in Stern et al. (1995; hereafter S95). We apply their results on homogeneous slab coronae to our average spectrum of RQ Seyfert 1s. The spectrum has $\alpha \simeq 0.9$ and the overall 2–18 keV spectral index, $\alpha_{2-18} \simeq 0.7$ (including the reflection component). For that α_{2-18} and assuming a pure e^\pm corona, S95 obtain $\tau \simeq 0.05$ and $kT \simeq 330$ keV (roughly corresponding to $E_c \simeq 500$ keV) in agreement with E_c obtained from our fits, see Table 1. This agreement supports the dissipative corona model of Haardt & Maraschi (1993).

On the other hand, Haardt, Maraschi & Ghisellini (1994) point out that since the UV fluxes in many Seyfert 1s are much larger than the X-ray fluxes (Walter & Fink 1993) the model of Haardt & Maraschi (1993), with most of the dissipation occurring in the corona, is ruled out. In that model, the UV emission is due to reprocessing of the X γ emission directed towards the cold disk, and EF_E in the UV and in X-rays are expected to be of the same order of magnitude. To the contrary, $EF_E(1375 \text{ \AA})/EF_E(2 \text{ keV})$ [from the best-fit values in Walter & Fink (1993)] for our RQ sample equals 0.8, 36, 0.2, 4.2, 19, 17, and 12 for MCG 8-11-11, NGC 3783, MCG -6-30-15, NGC 5548, ESO 141-G55, NGC 7469, and Mrk 509, respectively. We see that the ratio is > 10 for 4 objects. These large ratios can be explained if the corona is patchy rather than homogeneous and the corona dissipation dominates the disk dissipation only in the vicinity of an active region (a ‘patch’), but not globally (Haardt et al. 1994).

We also point out that a pure e^\pm pair corona would not form a thin slab above the disk surface (which was assumed by Haardt & Maraschi 1993). Hydrostatic equilibrium implies $H_c/R_d = (2r\Theta)^{1/2}$ for a pure pair, gas pressure-dominated, corona, where H_c is the corona scale-height, R_d is the disk radius, $r \equiv R_d c^2/(2GM)$, and $\Theta \equiv kT/(m_e c^2)$. Thus, $H_c/R_d \gtrsim 1$ for $\Theta \gtrsim 1$ and the assumption of a slab geometry breaks down.

S95 also provide one more argument against homogeneous slab coronae based on pair equilibrium. They calculate the maximum local compactness, $\ell_1 \equiv L_1 \sigma_T / (H_c m_e c^3)$, at which the homogeneous corona can be in pair equilibrium. Here L_1 is the luminosity from a characteristic local volume, H_c^3 , in the corona. For $\alpha_{2-18} \simeq 0.7$ of the *Ginga*/OSSE sample, S95 obtain $\ell_1 \lesssim 0.4$. The maximum value is achieved in a pure pair corona, and a presence of ionization electrons lowers the equilibrium value of ℓ_1 . S95 point out that this is in conflict with the AGN variability data (Done & Fabian 1989). On the other hand, S95 show that higher ℓ_1 are possible for patchy coronae. For $\alpha_{2-18} \simeq 0.7$ of the *Ginga*/OSSE sample, $\ell_1 \lesssim 15$ for an active region in the form of a hemisphere. That compactness appears compatible with the compactnesses estimated from X-ray variability (Done & Fabian 1989). The plasma parameters of RQ Seyfert 1s implied by thermal Comptonization are $\tau \simeq 0.2$ and $kT \simeq 0.7$ MeV in the case of pure pairs (see Fig. 1 in S95), which kT is compatible with our fitted values of E_c .

However, we point out that the results of S95 need to

be modified to account for the difference between the local compactness (used to compute pair equilibria) and the global compactness, $\ell \equiv L \sigma_T / (R_d m_e c^3)$ (where R_d is the radius of the region where the X γ luminosity L is produced). The latter (rather than the former) compactness is constrained from the variability data by $R_d \lesssim c \Delta t$ (Done & Fabian 1989). Using the formalism of Svensson & Zdziarski (1994) for the scale-height of the corona, assuming $\Theta \simeq 0.5$, and using the constraint on the size of the X-ray producing region of $r \lesssim 20$ (Tanaka et al. 1995; Fabian et al. 1994; Mushotzky et al. 1995), we obtain $\ell \gtrsim 40(1 + n_+/n_p)^{-1/2} \ell_1$. Thus, $\ell \gg \ell_1$ is possible in coronae. This largely resolves the conflict between the small local compactness required by pair equilibrium in a homogeneous corona and the variability data. Thus, the main argument against homogeneous coronae remains the large UV fluxes (Haardt et al. 1994), rather than pair production (S95).

More evidence against homogeneous coronae in Seyfert 1s is, however, provided by X-ray variability. Czerny & Lehto (1996) find that some variability light-curves from *EXOSAT* are truly stochastic rather than due to a deterministic chaos, which implies X-ray emission by multiple active centers rather than by a single extended source.

We note that studies of thermal pair plasmas in pair equilibrium predict no distinct pair annihilation even from a pair-dominated plasmas (Maciołek-Niedźwiecki, Zdziarski & Coppi 1995). A future detection of such a feature would indicate the plasma is either nonthermal with a hard electron injection (see Section 5.2) or there is a strong pair wind and pair annihilation takes place in a region spatially different from the hot corona (e.g., Maciołek-Niedźwiecki et al. 1995).

5.2 Nonthermal models

In nonthermal models, electrons are accelerated to or injected with a nonthermal distribution extending to relativistic energies. The electrons Compton upscatter UV seed photons to the X γ energy range, and the γ -rays may produce relativistic pairs, supplementing the primary injection of nonthermal electrons. We use here a numerical model of Lightman & Zdziarski (1987) with modifications given in Zdziarski, Coppi & Lamb (1990). We also take into account Compton reflection and absorption, which best-fit parameters for models below are almost the same as for the cut-off power-law model, Section 4. We fit the *Ginga*/OSSE data only since they provide more stringent constraints on the continuum parameters than the *EXOSAT*/OSSE data (see Section 4).

The simplest nonthermal model consists of power law electrons with the steady-state index of $p = 2\alpha + 1 \simeq 2.8$ that singly-scatter some soft seed photons in the Thomson regime, yielding a power-law photon distribution with $\alpha \simeq 0.9$ and a high-energy cutoff at $E \gg 511$ keV (Blumenthal & Gould 1970). If the relativistic electrons lose energy in the Thomson regime and thermalize within the source, the index, p , corresponds to injection of relativistic electrons with an index less by one (Blumenthal & Gould 1970), $\Gamma \simeq 2\alpha \simeq 1.8$. Since the model gives no high-energy cutoff in the hundred-keV range, it fits our data worse than the thermal model (represented by a cut-off power law, Section 3).

The best fit of such a model to the *Ginga*/OSSE data

shown by the solid curve in Fig. 3a corresponds to a low non-thermal compactness, $\ell = 0.1$ (implying negligible e^\pm pair production), the compactness in blackbody photons 20 times the nonthermal compactness (assuring that the X γ spectrum is entirely due to the first-order Compton scattering), and the best-fit $\Gamma = 1.85$. We see that the model is above the data at ~ 150 – 350 keV, which results in $\Delta\chi^2 = +4$ with respect to the thermal model. Increasing the nonthermal compactness steepens the X γ spectrum (Svensson 1987; Lightman & Zdziarski 1987) and further worsens the fit. E.g., $\ell = 20$, $\Gamma = 1.8$ yield $\Delta\chi^2 = +8$ with respect to the thermal model. Thus, we reject the ($\Gamma = 1.8$)-injection model.

On the other hand, Zdziarski et al. (1990) have proposed that the X-ray spectral index of $\alpha \simeq 0.9$ – 1 of Seyfert 1s is due to a nonthermal model with dominant pair production. The primary electrons are injected monoenergetically, which implies $\alpha = 0.5$ in the absence of pair production (Blumenthal & Gould 1970). Then, saturated nonthermal pair production yields the X-ray spectral index of $\alpha \simeq 1$ in the limit of $\ell \gg 10$ (Svensson 1987; Lightman & Zdziarski 1987), which can explain the X-ray spectra of Seyfert 1s. However, this model also predicts a steepening of the spectrum at a few tens of keV due to downscattering of hard X-rays and soft γ -rays by thermalized, optically thick, pairs (Sunyaev & Titarchuk 1980). This model was ruled out for IC 4329A by Z94, which conclusion we extend here to the average Seyfert-1 spectra. The dotted curve in Fig. 3a shows the best fit of this model ($\ell \simeq 30$). We see that the model lies below the ~ 50 – 150 keV spectrum, which results in an unacceptable $\Delta\chi^2 = +25$ with respect to the best-fit thermal model.

However, we find that some nonthermal models intermediate between the two models rejected above fit our data satisfactorily (as also shown by Z94 for IC 4329A). We consider here models with a power-law electron injection (between the Lorentz factors of 1.3 and 10^3), pair production, and allowing for repeated Compton scattering. This yields $\Gamma = 5.0_{-3.6}^{+4.4}$ with the same χ^2 as for the thermal model. The spectrum of the best-fit model ($\ell \simeq 130$; the solid curve in Fig. 3b) is due to repeated Compton upscattering by both the nonthermal and the thermal parts of the electron/pair distribution (Zdziarski et al. 1990; Ghisellini, Haardt & Fabian 1993). Note the similarity of the spectrum to that of the thermal model (Fig. 1). This nonthermal model yields no distinct pair-annihilation feature. The annihilation feature becomes stronger with decreasing Γ , illustrated by the dotted curve in Fig. 3b for $\Gamma = 2.5$ ($\ell \simeq 30$; $\Delta\chi^2 = +1.6$). Note that the annihilation features in Fig. 3a, b are allowed the OSSE data and do not constrain the models by themselves. Decreasing Γ also decreases the importance of repeated Compton upscattering. The spectrum for the lowest allowed Γ ($= 1.4$) is dominated by the first-order nonthermal Compton scattering by both the injected nonthermal electrons and nonthermal pairs (which pairs steepen the X-ray spectrum from $\alpha = \Gamma/2 = 0.7$ to the observed value of $\alpha = 0.9$).

6 CONCLUSIONS

We have obtained the average spectral parameters of RQ Seyfert 1s in X-rays and γ -rays based on samples of ob-

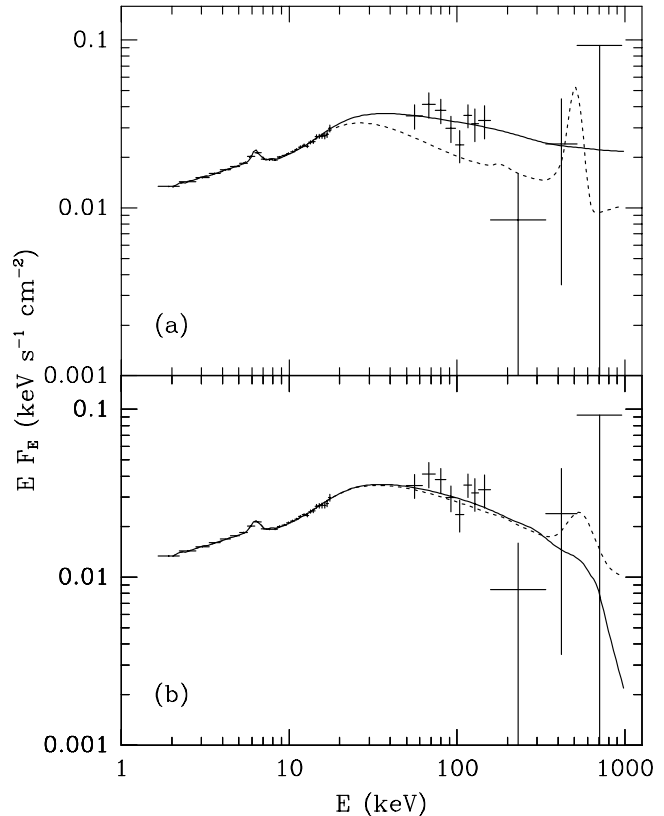


Figure 3. The average spectrum of RQ Seyfert 1s from *Ginga* and OSSE modeled by nonthermal plasmas. (a) Two examples of rejected models. The solid curve corresponds to a model with power-law electrons injected with the index $\Gamma = 1.85$ and with negligible both pair production and repeated Compton scattering. The dotted curve corresponds to a model with monoenergetic injection of electrons and a saturated pair cascade (Zdziarski et al. 1990). (b) Nonthermal models with power-law injection of electrons, providing fits as good as the best-fit thermal model. The solid curve represents the best-fit model with $\Gamma = 5.0$ and negligible pair production. The dashed curve represents a model with $\Gamma = 2.5$ and moderate pair production. See Section 5.2.

jects observed by both *Ginga* and OSSE and by both *EXOSAT* and OSSE. The estimates of the average spectrum from both samples are fully consistent with each other. Furthermore, they are consistent with the results of *HEAO-1* A1 and A4. The average spectrum contains an underlying power law with $\alpha \simeq 0.9$. There is also a Compton-reflection spectral component corresponding to cold matter covering a solid angle of $\sim 1.5\pi$ as seen from the X γ source. The power law continues to soft γ -rays and it breaks or it is cut off with an e -folding energy of $\gtrsim 250$ keV. The range of the e -folding energy obtained for our average spectra is fully consistent with that of IC 4329A (Z94; Madejski et al. 95). The average e -folding energy is *not* 40–50 keV, which was reported earlier based on the OSSE data alone.

Our average spectrum agrees well in X-rays with the average spectrum of all Seyfert 1s observed by *Ginga* (NP94). The intrinsic dispersion in the spectral index and the contribution of reflection in Seyfert 1s is given by NP94. On the other hand, the limited statistics of our OSSE spectra

allows us to provide only the range of the e -folding energy for the average spectrum with $\alpha = 0.90 \pm 0.05$. The value of the e -folding energy in individual AGNs appears to correlate positively with the X-ray spectral index (Zdziarski et al. 1996).

The average spectra of RQ Seyfert 1s can be modeled by Comptonization models with either thermal or nonthermal electrons. The Comptonizing plasma in thermal models is optically thin and relativistic. The plasma is likely to form a patchy corona above the surface of an accretion disk. Some models with relativistic nonthermal electrons predict the presence of an annihilation feature around 511 keV, which can be tested in the future by the *INTEGRAL* observatory (Winkler 1994).

ACKNOWLEDGEMENTS

This research has been supported in part by the Polish KBN grants 2P03D01008 and 2P03D01410, NASA grants, and the NSF grant PHY94-07194. It has made use of data obtained through the High Energy Astrophysics Science Archive Research Center Online Service, provided by NASA/GSFC. We are grateful to L. Angelini, C. Done, and R. Svensson for valuable discussions, and R. Cameron for letting us to use his data on NGC 7469 from OSSE. IMG acknowledges the financial support of the Universities Space Research Association.

REFERENCES

- Anders E., Ebihara M., 1982, *Geochim. Cosmochim. Acta*, 46, 2363
- Anders E., Grevesse N., 1989, *Geochim. Cosmochim. Acta*, 53, 197
- Antonucci R. R. J., 1993, *ARA&A*, 31, 473
- Arnaud K. A., 1996, in Jacoby G., Barnes J., eds, *Astronomical Data Analysis Software and Systems V*. The Astron. Soc. of Pacific, in press
- Bałucińska-Church M., McCammon D., 1992, *ApJ*, 400, 699
- Blumenthal G. R., Gould R. J., 1970, *Rev. Mod. Phys.*, 42, 237
- Czerny B., Lehto H. J., 1996, *MNRAS*, submitted
- Done C., Fabian A. C., 1989, *MNRAS*, 240, 81
- Fabian A. C., et al., 1994, *PASJ*, 46, L59
- George, I. M., Fabian, A. C., 1991, *MNRAS*, 249, 352
- Ghisellini G., Haardt F., Fabian A. C., 1993, *MNRAS*, 263, L9
- Haardt F., Maraschi L., 1993, *ApJ*, 413, 507
- Haardt F., Maraschi L., Ghisellini G., 1994, *ApJ*, 432, L95
- Johnson W. N., et al., 1994, in Fichtel C. E., Gehrels N., Norris, J. P., eds., *The Second Compton Symposium*. AIP, New York, p. 515
- Kaastra J. S., Mewe R., 1993, *A&AS*, 97, 443
- Krolik J. H., Kallman T. R., 1984, *ApJ*, 286, 366
- Lampton M., Margon B., Bowyer S., 1976, *ApJ*, 208, 177
- Lightman A. P., White T. R., 1988, *ApJ*, 335, 57
- Lightman A. P., Zdziarski A. A., 1987, *ApJ*, 319, 643
- Lin Y. C., et al., 1993, *ApJ*, 416, L53
- Maciutek-Niedźwiecki A., Zdziarski A. A., Coppi P. S., 1995, *MNRAS*, 276, 273
- Majejski G. M., et al., 1995, *ApJ*, 438, 672
- Magdziarz P., Zdziarski A. A., 1995, *MNRAS*, 273, 837
- Maisack M., et al., 1995, *A&A*, 298, 400
- Maisack M., Wood K. S., Gruber D. E., 1994, *A&A*, 284, 28
- Miyoshi S., et al., 1988, *PASJ*, 40, 127
- Mushotzky R. F., 1984, *Adv. Sp. Res.*, 3(10-12), 157
- Mushotzky R. F., et al., 1995, *MNRAS*, 272, L9
- Nandra K., Pounds K. A., 1994, *MNRAS*, 268, 405 (NP94)
- Pounds K. A., Nandra K., Stewart G. C., George I. M., Fabian A. C., 1990, *Nat*, 344, 132
- Reilman R. F., Manson S. T., 1979, *ApJS*, 40, 815
- Rothschild R. E., Mushotzky R. F., Baity W. A., Gruber D. E., Matteson J. L., Peterson L. E., 1983, *ApJ*, 269, 423
- Stern B. E., Poutanen J., Svensson R., Sikora M., Begelman M. C., 1995, *ApJ*, 449, L13 (S95)
- Sunyaev R. A., Titarchuk L. G., 1980, *A&A*, 86, 121
- Svensson R., 1987, *MNRAS*, 227, 403
- Svensson R., Zdziarski A. A., 1994, *ApJ*, 436, 599
- Tanaka Y., et al., 1995, *Nat*, 375, 659
- Turner M. J. L., et al., 1989, *PASJ*, 41, 345
- Turner T. J., Pounds K. A., 1988, *MNRAS*, 232, 463
- Turner T. J., Pounds K. A., 1989, *MNRAS*, 240, 833
- Walter R., Fink H. H., 1993, *A&A*, 274, 105
- Weaver K. A., Arnaud K. A., Mushotzky R. F., 1995, *ApJ*, 447, 121
- Wilkes B. J., Elvis, M., 1987, *ApJ*, 323, 243
- Winkler C., 1994, *ApJS*, 92, 327
- Wood K. S., et al., 1984, *ApJS*, 56, 507
- Woźniak P., et al., 1996, in preparation
- Zdziarski A. A., Coppi P. S., Lamb D. Q., 1990, *ApJ*, 357, 149
- Zdziarski A. A., Fabian A. C., Nandra K., Celotti A., Rees M. J., Done C., Coppi P. S., Madejski G. M., 1994, *MNRAS*, 269, L55 (Z94)
- Zdziarski A. A., Ghisellini G., George I. M., Svensson R., Fabian A. C., Done C., 1990, *ApJ*, 363, L1
- Zdziarski A. A., Johnson W. N., Done C., Smith D., McNaron-Brown K., 1995, *ApJ*, 438, L63 (Z95)
- Zdziarski A. A., Johnson W. N., Magdziarz P., 1996, *MNRAS*, in press